RESEARCH ARTICLE
ATMOSPHERIC PHYSICS

Earth and Planetary Physics
7: 675–683, 2023
doi: 10.26464/epp2023085

A comparative study of the electrical characteristics of positive and negative narrow bipolar events

FeiFan Liu[1,2,3], BaoYou Zhu[1*], HeLin Zhou[4], GaoPeng Lu[1,5], Ming Ma[1], and JiuHou Lei[1,2,3]

[1]CAS Key Laboratory of Geospace Environment, School of Earth and Space Sciences, University of Science and Technology of China, Hefei 230026, China;

[2]Mengcheng National Geophysical Observatory, University of Science and Technology of China, Hefei 230026, China;

[3]CAS Center for Excellence in Comparative Planetology, Hefei 230026, China;

[4]Provinn AB, Gothenburg, Sweden;

[5]Key Laboratory of Atmospheric Optics, Anhui Institute of Optics and Fine Mechanics, HFIPS, Chinese Academy of Sciences, Hefei 230026, China

Key Points:

- Using an improved transmission line model, we compare the electrical parameters of negative and positive NBEs (narrow bipolar events) and identify important differences between them.
- Negative NBEs generally produce narrower current pulses and shorter current traversal times than their positive counterparts.
- Negative NBEs tend to produce larger peak current moments but are associated with smaller charge moments than positive NBEs.

Citation: Liu, F. F., Zhu, B. Y., Zhou, H. L., Lu, G. P., Ma, M., Lei, J. H. (2023). A comparative study of the electrical characteristics of positive and negative narrow bipolar events. *Earth Planet. Phys.*, *7*(6), 675–683. http://doi.org/10.26464/epp2023085

Abstract: Narrow bipolar events (NBEs) are intriguing intra-cloud discharge that have attracted enormous interest in the lightning community. They come with two polarities that dominate at different altitudes in thunderclouds. The sources of negative NBEs are usually located near the top of thunderclouds; those of positive NBEs are at the middle levels. NBEs may occur at the onset of lightning. The electrical properties of NBEs remain poorly understood. We present here the first comparative study of the electrical characteristics of negative and positive NBEs. To derive electrical parameters from the fast electric field change waveforms of 1673 positive NBEs and 364 negative NBEs recorded by the Jianghuai Area Sferic Array (JASA) in China, we use an improved method based on the transmission line model. This approach concludes that negative NBEs occurring at high altitudes tend to produce a narrower current pulse and take a shorter time to traverse the channel than their positive counterparts. Moreover, compared to positive NBEs, a larger portion of negative NBEs are associated with slightly greater peak current moments but smaller overall charge moments. The differences reported herein between electrical properties of negative and positive NBEs suggest that charge distribution in NBE-producing thunderstorms tends to vary systematically with altitude.

Keywords: lightning; thunderstorm; narrow bipolar events

1. Introduction

Narrow bipolar events (NBEs), also named compact intra-cloud discharges (CIDs), refer to a distinct class of intra-cloud (IC) discharges that produce the strongest very high frequency (VHF) signals in nature, as well as energetic, narrow (10–30 μs) bipolar pulses in very low-frequency (VLF) and low frequency (LF) bandwidths. NBEs have received extensive attention in the lightning-studies community (Le Vine, 1980; Smith et al., 1999; Jacobson et al., 2005; Wiens et al., 2008; Nag et al., 2010; Rison et al., 2016; Tilles et al., 2019). Recent measurements from space by the Atmosphere–Space Interactions Monitor (ASIM) suggest that NBEs are corona discharges that are associated with blue emissions at 337 nm with weak or no detectable emissions at 777.4 nm (Liu FF et al., 2021a; Li DS et al., 2021; Soler et al., 2020). In this work we use the NBE terminology because we have selected for study discharges characterized by narrow VLF/LF waveform features.

NBEs are divided into two polarities that originate at different altitudes in thunderclouds (e.g., Willet et al., 1989; Zhu BY et al., 2010b; Wu T et al., 2011). Positive NBEs generally occur between the mid-level main negative charge layer and the upper positive charge layer (Wu T et al., 2011; Lü, FC et al., 2013). Positive NBEs usually occur in isolation; they can also serve as precursors of normal IC flashes (Wu T et al., 2012; Leal and Rakov, 2019; Lyu FC et al., 2019; Bandara et al., 2020). Negative NBEs usually occur between the main positive charge layer and the screening charge layer at the top of an extremely vigorous thundercloud (Wu T et al., 2013; Liu FF et al., 2021b); they also can be observed in the low region (Bandara et al., 2019). Negative NBEs can trigger blue discharges, a type of upward lightning discharge emitting from

First author: F. F. Liu, feifan@ustc.edu.cn
Correspondence to: B.Y. Zhu, zhuby@ustc.edu.cn
Received 26 JUL 2023; Accepted 28 SEP 2023.
First Published online 10 NOV 2023.

the thundercloud top (Chanrion et al., 2017; Liu FF et al., 2018; Chou et al., 2018; Neubert et al., 2021).

Because NBEs occur inside thunderclouds, it is relatively difficult to measure their electrical parameters directly. Some researchers have estimated the electrical parameters of NBEs by making physical assumptions based on signatures of sferic waveforms detected at single stations, or on combinations of such waveforms detected by stations near and far (Smith et al., 1999; Eack, 2004; Watson and Marshall, 2007; Nag and Rakov, 2010a, 2010b; Zhu BY et al., 2010a). Karunarathne et al. (2016) used electric field (*E*-field) changes measured at multiple stations to estimate the dipole charge moments of 10 positive NBEs, ranging from 0.46 C·km to 1.81 C·km. By viewing an NBE as the electromagnetic transient related to the rapid elongation of the negative leader tip in the ambient thunderstorm electric field (*E*-field), da Silva and Pasko (2015) proposed a unified physical mechanism to reproduce the NBE's bipolar waveform under the assumed electrical properties.

Exploiting the high resolution of broadband interferometers, Liu HY et al. (2012) used two broadband very-high-frequency (VHF) interferometers to map the three-dimensional geometry of 11 NBEs. They estimated that the channel of an NBE develops mainly in the vertical direction over an extent 0.40–1.9 km with mean apparent extending speed of 0.61×10^8 m/s. and mean speed of the current wave in the NBE channel of 1.4×10^8 m/s. Rison et al. (2016) presented the downward expansion of VHF sources for 3 positive NBEs by combining data from a broadband VHF interferometer and the New Mexico Tech 3D Lightning Mapping Array (LMA). Also, the extent (~500 m) and extending speed (~0.4–0.5×10^8 m/s) of VHF sources inferred from VHF data have been used to estimate the current peak and amount of charge transfer in an NBE, from measured *E*-field waveforms at close ranges.

The aforementioned analyses of the electrical properties of NBEs have been focused mainly on limited case studies. In particular, studies of the electrical parameters of negative NBEs on the cloud top are lacking. In this work, we present a statistical comparison of the electrical characteristics of negative and positive NBEs. A current waveform retrieval model is used to estimate, based on distant *E*-field waveforms, the following electrical parameters of NBEs: current traversal time, current waveform width, peak current moment, and charge moment.

2. Methodology

The method used in this work is adapted from the transmission line model of Zhu BY et al. (2010a). Compared with previous models, the present model applies the complete *E*-field waveform, rather than the initial half cycle, to estimate the time for an NBE current pulse to reach the top of the channel, and to capture the pulse's temporal characteristics. Figure 1 illustrates the geometry of an NBE discharge. The NBE channel with length l is vertically oriented at height h above the assumed perfectly-conducting ground.

When a time-varying current pulse $I(t)$ is injected at one end of the channel and propagates without distortion along the channel at a constant speed v, the *E*-field waveform at a distance $r \gg h$ is derived as follows (Rakov and Uman, 2003):

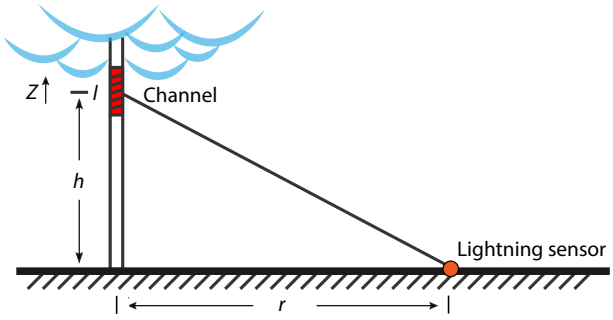

Figure 1. Schematic diagram for calculating the electrical field of an NBE discharge with channel length l and central height h from data collected at distance r.

$$E(r,t) = \frac{v}{2\pi\varepsilon_0 c^2 r}\left[I(t - r/c) - I(t - \Delta t - r/c)\right], \tag{1}$$

where c is the speed of light in air and ε_0 is the air permittivity. The term $\Delta t = l/v$ presents the current traversal time and is critically related to the channel length. By using the substitution $v = l/\Delta t$, Equation (1) can be rewritten in terms of the current moment $M(t) = lI(t)$ as:

$$E(r,t) = \frac{1}{2\pi\varepsilon_0 c^2 r\Delta t}\left[M(t - r/c) - M(t - \Delta t - r/c)\right], \tag{2}$$

which indicates that the distant *E*-field depends on the current moment waveform and the current traversal time Δt. For simplicity, the current waveform is essentially described with two parameters: α and β as below (Oetzel, 1968).

$$I(t) = A\mathrm{e}^{-\alpha t}\left(\mathrm{e}^{\sqrt{\alpha^2-\beta^2}\,t} - \mathrm{e}^{-\sqrt{\alpha^2-\beta^2}\,t}\right), \tag{3}$$

where A, relating to the amplitude of the current waveform, is arbitrary within the framework of our model; thus, from the resultant single-station *E*-field waveform alone, one can uniquely determine only the amplitude of the current moment rather than that of the current itself (da Silva and Pasko, 2015). From Equations (2) and (3), we see that the distant *E*-field waveform is governed jointly by three variables (α, β, and Δt), in that favorable values of these variables are expected to produce an *E*-field waveform that is a good match to the observed *E*-field.

We try a series of values for α, β and Δt to find the best match between modeled and observed *E*-field waveforms. The parameter α is assumed to vary in the range of 0.05–1.0 μs^{-1} with increments of 0.002; parameter β ranges between 0.05 and 1.0 μs^{-1} in steps of 0.002; parameter Δt is assigned values between 1.0 and 15 μs at intervals of 0.1 μs. α_i is the i^{th} value in the range of α; β_j is the j^{th} value in the β range; Δt_k is the k^{th} value in the Δt range. A computational code was developed to calculate, first, following Equation (3), the current waveform with arbitrary amplitudes for values of α_i and β_j, and then, following Equation (2), to calculate the resultant distant *E*-field by current propagation at speed Δt_k.

The calculated *E*-field is then compared to the observed *E*-field to assess the fit between the two waveforms. We define the matching degree (MD) between the simulated and observed *E*-field waveform during the entire duration T as follows:

$$\mathrm{MD}(i,j,k)=\int_0^T\left(\mathrm{UE}_m\left(t,\alpha_i,\beta_j,\Delta t_k\right)-\mathrm{UE}_O(t)\right)^2\mathrm{d}t, \tag{4}$$

where UE_m (t, α_i, β_j, Δt_k) denotes the calculated *E*-field waveform normalized to unity amplitude, and $\mathrm{UE}_O(t)$ presents the observed *E*-field normalized to unity amplitude. The parameters of α, β and Δt are chosen to minimize the value of MD, based on the limited values of α, β and Δt mentioned before. As shown in Equation (2), once the quantity of Δt is determined, the amplitude (peak) of current moment is fixed accordingly.

It is worth noting that the propagation attenuation of *E*-field waveform over a finitely conducting path is also considered before the fit. The Fourier transform is applied to the simulated *E*-field (under the assumption of a perfectly conducting ground) to obtain each frequency component. The attenuation function, which describes the attenuation factor at each frequency of interest, is multiplied by each frequency component. Finally, an inverse Fourier transform is performed to obtain the *E*-field in the time domain. The attenuation function is similar to the attenuation factor of an elevated dipole above ground used by Cooray (2007); we choose the ground conductivity to be 0.001 S/m.

3. Experiment and Data

The *E*-field waveforms of the NBEs examined in this work were obtained from the Jianghuai Area Sferic Array (JASA), a GPS-based multi-station network that can continuously record lightning signals at a sampling rate of 5 MHz/s with a bandwidth of 800 Hz–400 kHz (Qin ZL et al., 2015; Liu FF et al., 2018). The timing accuracy at individual stations is better than 50 ns. In the post-processing of lightning signals, a waveform recognition algorithm was applied to identify an NBE (Ma D, 2017; Liu FF et al., 2018). Each NBE was synchronously detected at four or more stations. From those data, a time-of-arrival technique was used to obtain the two-dimensional location of the event. Its source height was estimated by calculating the time differences between the ground wave and the paired ionosphere reflections (Smith et al., 2004; Liu FF et al., 2018).

Overall, we identified 411 negative NBEs and 1821 positive NBEs from four strong thunderstorms that occurred on July 4, July 6, July 7, and August 19, 2012. The thunderstorm on August 19 produced 253 negative NBEs, six of which have been reported by Liu FF et al. (2018), to demonstrate the close relationship between negative NBEs and blue discharges. The *E*-field waveforms recorded at the central VLF/LF station were used to estimate the electrical parameters of individual NBEs. We note that the overwhelming majority of NBE waveforms produce relevant MD values as small as several fractions, indicating a near-perfect fit between the simulated and observed *E*-field waveforms. However, when an NBE waveform is significantly influenced by fine structures on the overshoot portion (Hamlin et al., 2007), the MD value becomes larger. These fine structures are likely produced by current reflection at the channel extremity (Hamlin et al., 2007; Nag and Rakov, 2010a). As the current is absorbed in the end of the channel in our model, we have excluded NBEs with *E*-field waveforms significantly influenced by fine structures on overshoot (in particular, those with MD values larger than 6). This selection criterion left 364 negative and 1673 positive NBEs for analysis.

Leal et al. (2019) presents a comprehensive discussion of waveform classification of NBEs. They found that more than half of observed CIDs exhibited pronounced ringing on the opposite-polarity overshoot of their bipolar electric field waveforms, which is indicative of a bouncing wave process. As we show in Figure 2a, many of the NBE *E*-field waveforms in this study exhibit fine structures on overshoot. By excluding only those NBEs whose relatively large fine structures lead to MD bias values greater than 6, we ensure that

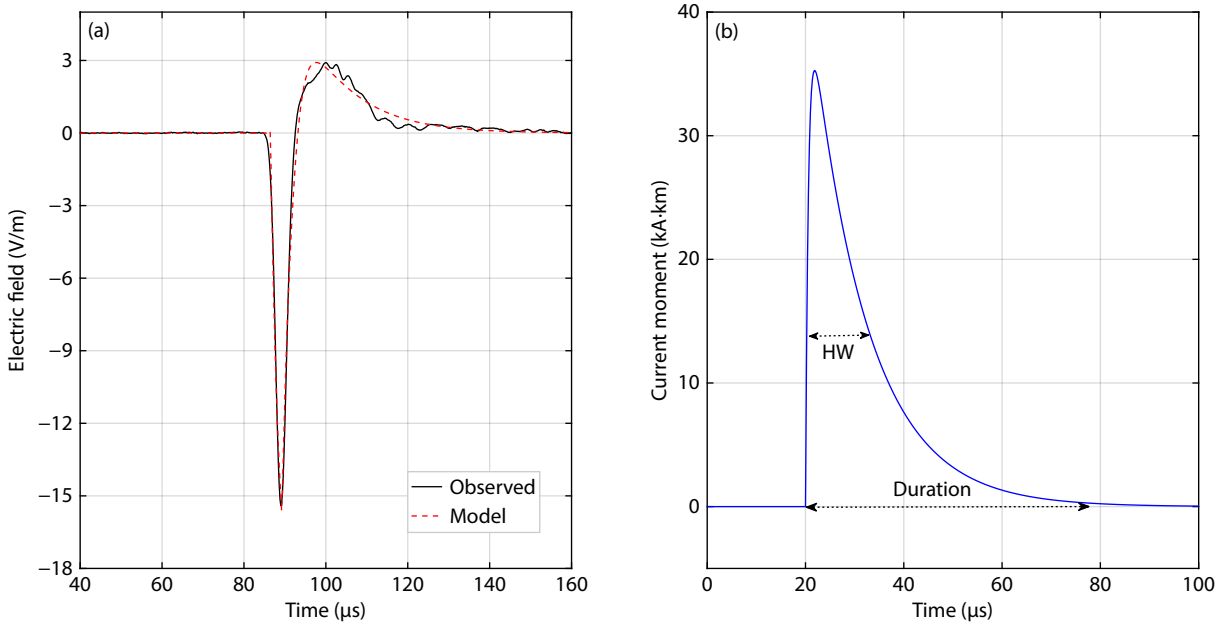

Figure 2. Model results for a positive NBE located at a height of 7.2 km, 150 km from a VLF/LF station. (a) Comparison between the measured *E*-field waveform (black solid line, normalized to 100 km *E*-field peak 15.4 V/m) and simulated *E*-field waveform (red dashed line). (b) Derived current moment waveform with $\alpha = 0.774\ \mu s^{-1}$, $\beta = 0.358\ \mu s^{-1}$; peak current moment is 35.3 kA·km.

our model-predicted waveforms fit well with the bulk of empirically-observed waveforms.

As an example, Figure 2 illustrates the model results for a positive NBE with noticeable, but not extreme, fine features on the overshooting portion of its *E*-field waveform. The model yields a fitness degree of MD = 4.6 for this NBE, corresponding to parameters $\alpha = 0.774$ μs^{-1}, $\beta = 0.358$ μs^{-1}, and $\Delta t = 2.7$ μs. The current moment waveform has a peak of 35.3 kA·km; the half-width of the initial peak (HW) is 10.3 μs, and the duration (from start to the time when the amplitude drops to 0.5% of peak) is 63 μs. We note that the above results were obtained under the assumed ground conductivity of 0.001 S/m. Altering the ground conductivity assumptions to 0.005 S/m (0.01 S/m) the model predicted peak current moments and current traversal times, respectively, of 31.4 kA·km (28.5 kA·km) and 2.7 μs (2.9 μs).

4. Results

In the following, we derive the electrical characteristics of 364 negative NBEs and 1673 positive NBEs based on the method described above. The output parameters (α, β, Δt, as well as the peak current moment) for each NBE are derived from the *E*-field waveform and are then used to build the data sets for electrical parameters, including each NBE discharge's current traversal time, current waveform width, peak current moment, and charge moment.

4.1 Current Traversal Time

The current traversal time (Δt) refers to the time for the current pulse to reach the other end of the channel; Δt can be retrieved from the NBE radiation waveform. Figure 3a shows the scatterplots of Δt versus the source height of NBEs. For the 364 negative NBEs, the Δt value averages 3.2 μs, which is significantly smaller than the mean of 4.3 μs for the 1673 positive NBEs. We see that Δt values for a few positive NBEs at relatively low altitudes in the cloud (~6–12 km) can exceed even 10 μs. However, Δt values for positive NBEs at relatively high altitudes in the cloud (>12 km) rarely exceed several microseconds, which is equivalent to Δt values for negative NBEs at the same height. Figure 3b directly compares the Δt distributions of negative and positive NBEs; the comparison reveals that the durations of negative NBEs tend to be shorter than those of positive NBEs.

By assuming that the current pulses reflect at the end of the channel and produce secondary peaks in the electric field change records, Hamlin et al. (2007) calculated the current traversal time (the time difference between the primary and secondary peaks in the field change record) for 133 out of 1115 positive NBEs. Their Δt values range from several microseconds to more than 10 microseconds, which is consistent with our work. Meanwhile, the mean Δt value (6.7 μs) reported by Hamlin et al. (2007) is larger than the mean value (4.3 μs) in this study. As discussed by Nag and Rakov (2010a), the measuring technique used by Hamlin et al. (2007) may lead to an overestimation of Δt. Rison et al. (2016) reported breakdown channel extension time intervals of 12 μs and 10 μs for two positive NBEs, values that are close to the upper limit of Δt values in this study and in that of Hamlin et al. (2007), but significantly larger than the average value (4.3 μs) of Δt reported in our work. Li DS et al. (2022) gave slightly different channel traversal times (L/v) — 13 and 16 μs for NBE1 and NBE3, respectively. Although NBE discharges are initiated by instances of fast positive breakdown and are associated with cold streamers (Rison et al., 2016; Liu FF et al., 2021a), it remains unclear whether the breakdown channel extension time measured from VHF sources is exactly equal to the current traversal time derived from electromagnetic field waveforms in VLF/LF bands.

4.2 Temporal Characteristics of the Current Waveform

As illustrated in Figure 2b, when quantities of α and β are derived from the *E*-field waveform of NBEs, the current waveform can be reproduced from Equation (3) for time characteristic quantities. We focus on the half-width and full duration of an NBE current

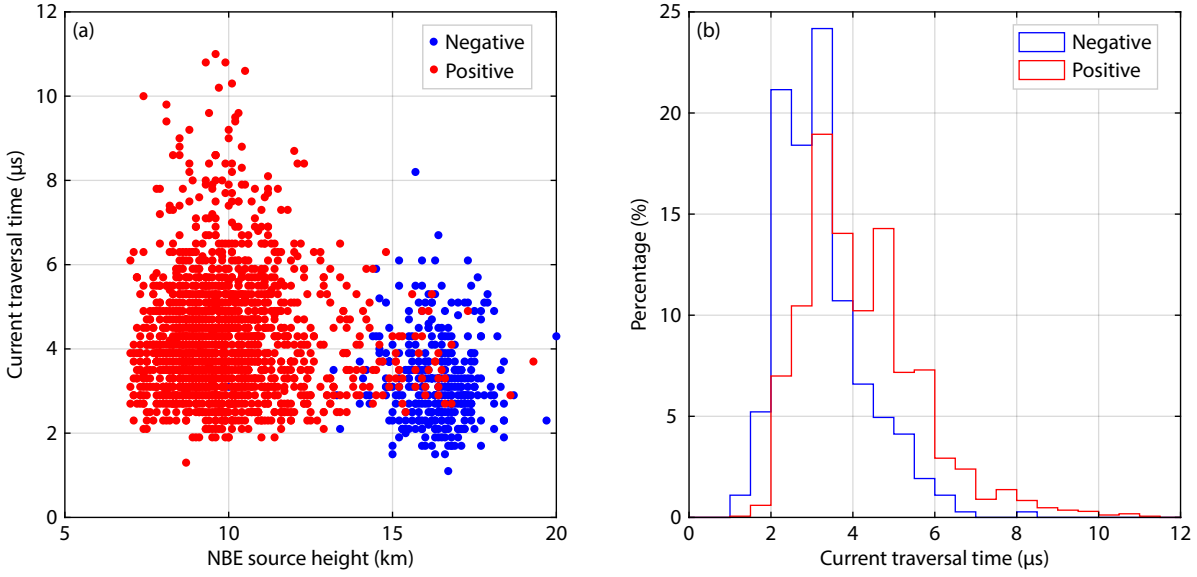

Figure 3. (a) Scatter diagrams of estimated current traversal time (Δt) versus source height, and (b) Histograms of Δt for negative and positive NBEs.

pulse (see Figure 2b). The scatter diagrams of half-width and full durations of NBE current waveforms versus their source heights are shown in Figures 4a and 4c, respectively. The histograms of half-width and full-width NBE current pulses are presented in Figures 4b and 4d, respectively. The half-width graphs exhibit normal distributions with means of 7.1 μs for negative NBEs and 8.6 μs for positive NBEs. The average current duration of positive NBEs (31.1 μs) is almost twice that of negative NBEs (17.5 μs). On average, negative NBEs produce current pulses that are much narrower and of shorter duration than the current pulses of positive NBEs. However, it is interesting to note that positive NBEs that originate at relatively higher heights exhibit similar current durations to those of negative NBEs.

Karunarathne et al. (2016) reported that the bipolar pulse of an NBE is followed by a relatively long, slow electrostatic change with a duration of several milliseconds or longer. To model the electrostatic change associated with an NBE, they proposed a current pulse composed of a brief breakdown current pulse and then a smaller prolonged current. We note that the "NBE current waveform" that we derive from the radiation field waveforms in our work includes only the main breakdown pulse described in Karunarathne et al. (2016) and Rison et al. (2016); it does not include the possible prolonged current that they include in their model.

4.3 Current Moment and Charge Moment

As illustrated in Equation (2), the peak current moment of an NBE can be retrieved directly from its radiation field waveform. Figure 5 presents the model-estimated distribution of peak current moment for negative and positive NBEs. For positive NBEs, the peak current moment ranges from 5.48 to 75.9 kA·km with median and mean values of 28.7 and 27.8 kA·km, respectively. Negative NBEs produce a similar median value (27.7 kA·km); however, a higher portion of negative NBEs produce large peak current moments (>60 kA·km) and their mean value (34.9 kA·km) is larger than that of positive NBEs, as illustrated in Figure 5b. Note (Figure 5a) that positive NBEs observed at relatively higher heights tend to avoid large current moments; at these higher altitudes, peak current moments of positive and negative NBEs are similar.

We also estimate the charge moment involved in an NBE through the time integral of the current moment $M(t)$ as $Q_{\mathrm{NBE}} = \int_0^T M(t)\,\mathrm{d}t$. The scatterplots of charge moment estimated for negative NBEs and positive NBEs are shown in Figure 6a. We see that both negative and positive NBEs produce charge moments of several tenths C·km. However, negative NBEs at relatively higher altitudes tend to produce a smaller minimum charge moment than positive NBEs at relatively lower altitudes, and the minimum NBE charge moment tends to decrease with height. The histogram of charge moment for the different NBE polarities, Figure 6b, shows a slightly larger average charge moment for positive NBEs (+0.27 C·km) than negative NBEs (−0.25 C·km). It is interesting to compare Figure 6b with Figure 5b; clearly, negative NBEs tend to produce smaller charge moments than positive NBEs.

Smith et al. (1999) estimated dipole charge moments from the radiation fields of 15 positive NBEs; they reported minimum and maximum values of 0.26 and 0.8 C·km, and a mean value of 0.38 C·km. Their estimated average current moment of the 15 positive NBEs, about 28 kA·km, is in quite good agreement with our value of about 27.8 kA·km (for 1673 positive NBEs). By close-range measurements of the electrostatic field changes, Eack (2004) estimated the charge moments for 5 positive and 2 negative NBEs ranging from 0.15 to 2.0 C·km. Based on electrostatic field changes measured at multiple close stations, Karunarathne et al. (2016) estimated the 3-D charge moment for 10 NBEs ranging

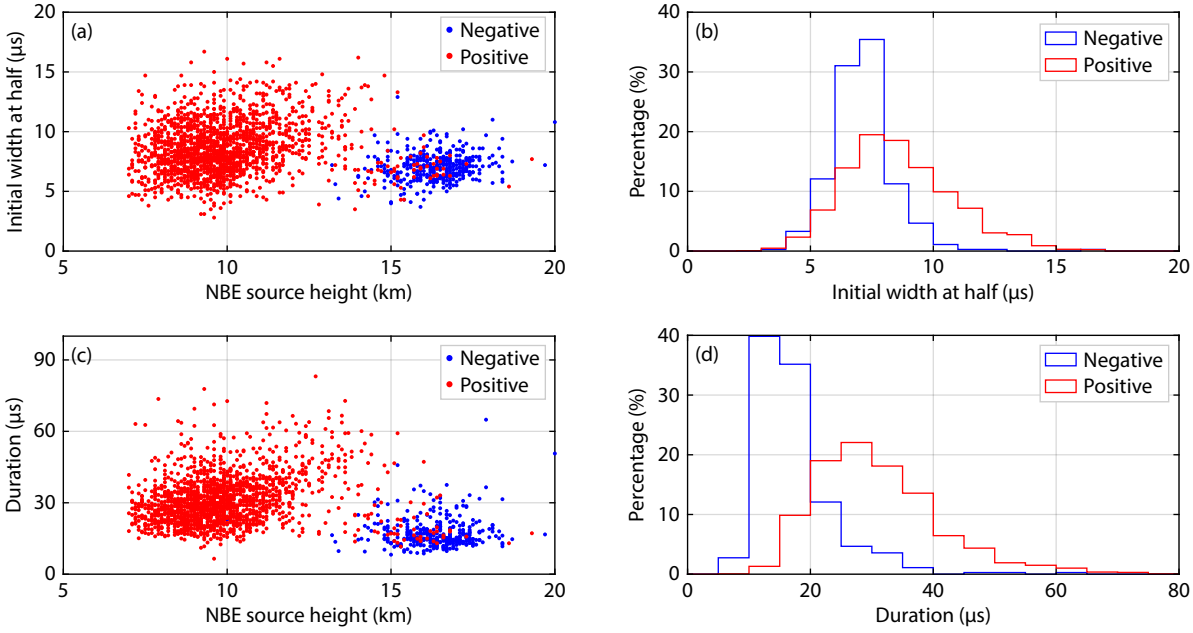

Figure 4. Derived waveform features for both polarities of NBEs. (a) and (b) Distributions of the initial width at half of the current waveform for both polarities of NBEs; (c) and (d) Distributions of the duration of the derived current waveform for NBEs.

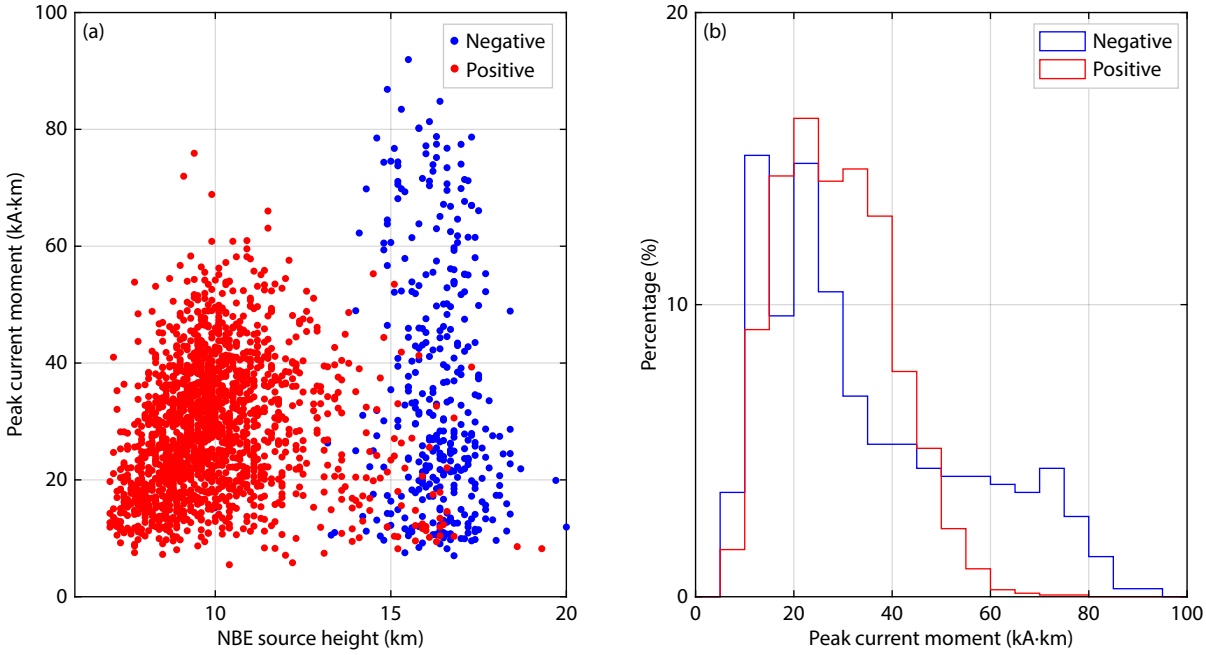

Figure 5. Derived peak current moment for both polarities of NBEs. (a) Scatterplots of peak current moment versus NBE source height; (b) histograms of peak current moment.

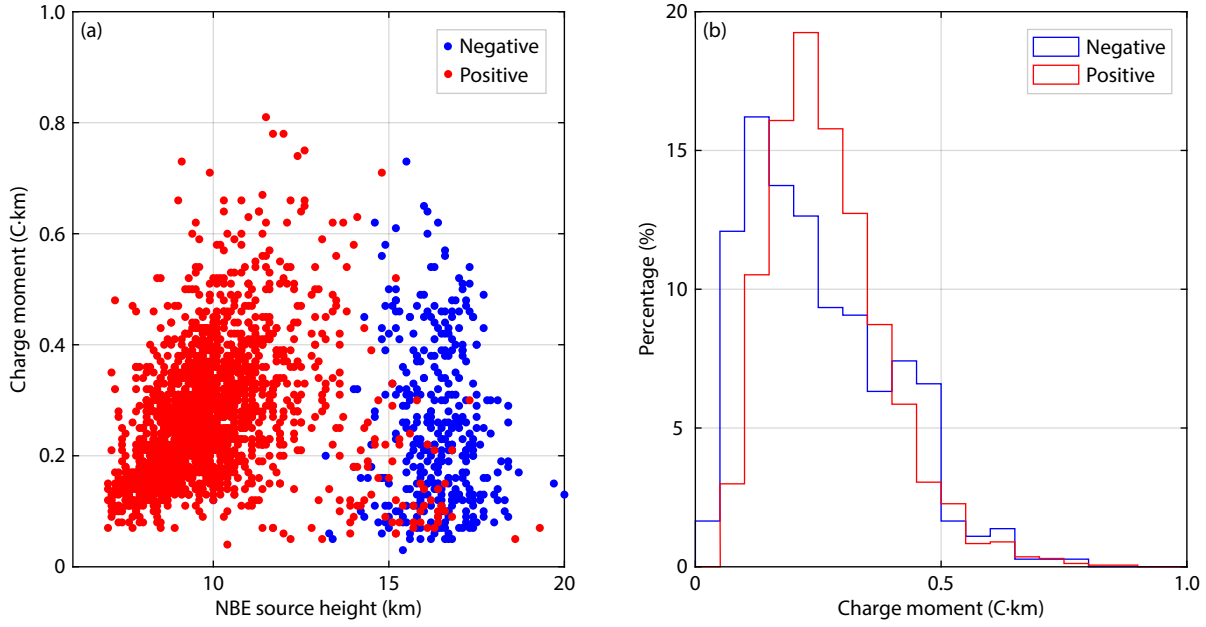

Figure 6. Derived charge moment for both polarities of NBEs. (a) Scatterplots of charge moment versus NBE source height, (b) histograms of charge moment.

from 0.46 to 1.81 C·km, with an average of 1.09 C·km; this value is about 3 times larger than the average charge moment (approximately +0.27 C·km for positive NBEs) reported in this study. It should be noted that our model estimates only the vertical component of the 3-D charge moment (tiled from vertical), not including the contribution of the slow charge transfer that is obvious in the slow NBE electrostatic change (Karunarathne et al., 2016). Rison et al. (2016) modeled the electrostatic field changes for 3 close NBEs whose vertical channels were mapped by VHF source location; they reported charge moments of about 0.09, 0.18, and 0.08 C·km, respectively. da Silva and Pasko (2015) and Watson and Marshall (2007) also modeled the radiation pulse of an NBE and reported a charge moment of several tenths of a C·km, which is reasonably within the range of our results.

5. Discussion

Table 1 summarizes our statistical results for the electrical features of positive and negative NBEs. We find that negative NBEs, which generally occur at relatively high thundercloud altitudes, tend to produce narrower current pulses than positive NBEs. The average half-width and full width of negative NBE current pulses are, respectively, 7.1 μs and 17.5 μs, compared to 8.6 μs and 31.1 μs for

Table 1. Electrical characteristics for positive and negative NBEs.

Parameter	−NBEs (364)		+NBEs (1673)	
	Mean (SD)	Min/Median/Max	Mean (SD)	Min/Median/Max
Current traversal time (Δt)	3.2 (1.0)	1.1/3.1/8.2	4.3 (1.4)	1.4/3.9/11.0
Half width of current (μs)	7.1 (1.3)	3.7/7.1/16.1	8.6 (2.2)	2.8/8.3/16.7
Duration of current (μs)	17.5 (6.4)	8.2/15.6/64.9	31.1 (10.3)	6.5/29.4/83.1
Peak current moment (kA·km)	34.9 (20.7)	7.02/27.7/92.0	28.7 (11.3)	5.48/27.8/75.9
Charge moment, Q_{NBE} (C·km)	0.25 (0.15)	0.03/0.22/0.76	0.27 (0.12)	0.04/0.25/0.87

positive NBEs. The average current traversal times (Δt) are 3.2 μs for negative NBEs and 4.3 μs for positive NBEs. These results suggest that negative NBE current pulses require shorter times to traverse the channel than do those of positive NBEs. The average peak current moment of negative NBEs (34.9 kA·km) is larger than that (28.7 kA·km) for positive NBEs; Figure 5b suggests that this difference is explained by the higher proportion of negative NBEs with large current moments. However, the charge moments of the positive and negative NBEs do not show a similar tendency.

We conjecture that the differences in electrical properties between negative and positive NBEs are likely to be explained by their charge distributions at different altitudes by convection strength (Rakov and Uman, 2003). Negative NBEs tend to occur in vigorous thunderstorms (Wu T et al., 2013, Liu FF et al., 2021c). Intense convection would lead to a stronger upper positive charge layer. This may serve as the abundant charge supply for negative NBEs above the upper positive charge layer. Furthermore, strong convection would be expected to lift the positive charge layer close to the screening charge layer attached to the cloud top, which would produce negative NBEs with shorter Δt values. The relatively extensive (less lumpy) positive charge regions tend to produce large current over the cross-sectional area as a volume current density (Rison et al., 2016), which may explain the relatively greater proportion of negative NBEs with large current moments, as seen in Figure 5.

Additionally, the protuberant negative charge lump is more likely to enhance the local electric field farther up the negative charge layer to initiate a downward positive NBE (Rison et al., 2016), which gives rise to the larger Δt values of positive NBEs at lower altitudes, as shown in Figure 3. The local charge lump would also constrain the available charge supply and prevent the extremely large current moment for positive NBEs at lower altitudes, as shown in Figure 6a. As the Δt value represents the quotient of the channel length divided by the current propagation speed during the NBE discharge, the significant difference in the distribution of Δt values between negative and positive NBEs suggests that they may differ in channel length (l) and current propagation speed (v). According to Rison et al. (2016), both positive and negative NBEs are initiated by fast positive breakdowns and show no significant difference in speed with altitude. Although we cannot rule out the possibility that negative NBEs have faster current propagation speeds than positive NBEs, the shorter current traversal times and the narrower current pulses observed for negative NBEs (Figures 3 and 4) suggest that negative NBEs are shorter in channel length than positive NBEs, which is likely caused by the narrower gap, between the upper positive charge layer and the screening charge layer, than the gap, in vigorous thunderstorms, between the upper positive charge and the main negative charge layer inside and below. More precise determination of channel properties will be required in future work, such as coordinated VHF source-mapping and VLF/LF radiation field waveform observations.

6. Conclusions

In summary, our study has compared the electrical parameters of NBEs of both polarities, from data collected during four thunderstorms in East China. From their *E*-field waveforms, we derived output parameters (α, β, Δt, as well as peak current moments) of 364 negative NBEs and 1673 positive NBEs and used these results to build data sets for the relevant NBE electrical parameters — current traversal time, current waveform width, peak current moment, and charge moment. Results are summarized as follows:

(1) Current traversal times of negative NBEs are generally shorter than those of positive NBEs. Some positive NBEs at relatively higher heights, however, do exhibit short current traversal times.
(2) Current pulses of positive NBEs tend to be wider than those of negative NBEs, but some positive NBEs, occurring at altitudes more typical of negative NBEs, exhibit current pulse durations more typical of negative NBEs.
(3) Compared to positive NBEs, a larger portion of negative NBEs are associated with relatively large peak current moments, but also with smaller charge moments.

Acknowledgments

The authors would acknowledge financial support from the National Key Laboratory on Electromagnetic Environmental Effects and Electro-optical Engineering (NO. JCKYS2022LD6), the National Natural Science Foundation of China (42005068 and 42375074), the Project of Stable Support for Youth Team in Basic Research Field CAS (YSBR-018), and the Joint Open Fund of Mengcheng National Geophysical Observatory (MENGO-202208).

References

Bandara, S., Marshall, T., Karunarathne, S., Karunarathne, N., Siedlecki, R., and Stolzenburg, M. (2019). Characterizing three types of negative narrow bipolar events in thunderstorms. *Atmos. Res.*, *227*, 263–279. https://doi.org/10.1016/j.atmosres.2019.05.013

Bandara, S., Marshall, T., Karunarathne, S., and Stolzenburg, M. (2020). Electric field change and VHF waveforms of Positive Narrow Bipolar Events in Mississippi thunderstorms. *Atmos. Res.*, *243*, 105000. https://doi.org/10.1016/j.atmosres.2020.105000

Chanrion, O., Neubert, T., Mogensen, A., Yair, Y., Stendel, M., Singh, R., and Siingh, D. (2017). Profuse activity of blue electrical discharges at the tops of thunderstorms. *Geophys. Res. Lett.*, *44*(1), 496–503. https://doi.org/10.1002/2016GL071311

Chou, J. K., Hsu, R. R., Su, H. T., Chen, A. B. C., Kuo, C. L., Huang, S. M., Chang, S. C., Peng, K. M., and Wu, Y. J. (2018). ISUAL-observed blue luminous events: the associated sferics. *J. Geophys. Res.: Space Phys.*, *123*(4), 3063–3077. https://doi.org/10.1002/2017JA024793

Cooray, V. (2007). Propagation effects on radiation field pulses generated by cloud lightning flashes. *J. Atmos. Sol. - Terr. Phys.*, *69*(12), 1397–1406. https://doi.org/10.1016/j.jastp.2007.03.009

da Silva, C. L., and Pasko, V. P. (2015). Physical mechanism of initial breakdown pulses and narrow bipolar events in lightning discharges. *J. Geophys. Res.: Atmos.*, *120*(10), 4989–5009. https://doi.org/10.1002/2015JD023209

Eack, K. B. (2004). Electrical characteristics of narrow bipolar events. *Geophys. Res. Lett.*, *31*(20), L20102, https://doi.org/10.1029/2004GL021117

Jacobson, A. R., and Heavner, M. J. (2005). Comparison of narrow bipolar events with ordinary lightning as proxies for severe convection. *Mon. Wea. Rev.*, *133*(5), 1144–1154. https://doi.org/10.1175/MWR2915.1

Karunarathne, S., Marshall, T. C., Stolzenburg, M., and Karunarathna, N. (2016). Electrostatic field changes and durations of narrow bipolar events. *J. Geophys. Res: Atmos.*, *121*(17), 10161–10174. https://doi.org/10.1002/2016JD024789

Hamlin, T., Light, T. E., Shao, X. M., Eack, K. B., and Harlin, J. D. (2007). Estimating lightning channel characteristics of positive narrow bipolar events using intrachannel current reflection signatures. *J. Geophys. Res: Atmos.*, 112(D14). https://doi.org/10.1029/2007JD008471

Le Vine, D. M. (1980). Sources of the strongest RF radiation from lightning. *J. Geophys. Res.: Oceans*, *85*(C7), 4091–4095. https://doi.org/10.1029/JC085iC07p04091

Leal, A. F. R., and Rakov, V. A. (2019). A study of the context in which compact intracloud discharges occur. *Sci. Rep.*, *9*(1), 12218. https://doi.org/10.1038/s41598-019-48680-6

Leal, A. F. R., Rakov, V. A., and Rocha, B. R. P. (2019). Compact intracloud discharges: new classification of field waveforms and identification by lightning locating systems. *Electr Power Syst. Res.*, *173*, 251–262. https://doi.org/10.1016/j.epsr.2019.04.016

Li, D. S., Luque, A., Gordillo-Vázquez, F. J., Liu, F. F., Lu, G. P., Neubert, T., Chanrion, O., Zhu, B. Y., Østgaard, N., and Reglero, V. (2021). Blue flashes as counterparts to narrow bipolar events: the optical signal of shallow in-cloud discharges. *J. Geophys. Res.: Atmos.*, *126*(13), e2021JD035013. https://doi.org/10.1029/2021JD035013

Li, D. S., Luque, A., Gordillo-Vázquez, F. J., da Silva, C., Krehbiel, P. R., Rachidi, F., and Rubinstein, M. (2022). Secondary fast breakdown in narrow bipolar events. *Geophys. Res. Lett.*, *49*(7), e2021GL097452. https://doi.org/10.1029/2021GL097452

Liu, F. F., Zhu, B. Y., Lu, G. P., Qin, Z. L., Lei, J. H., Peng, K. M., Chen, A. B., Huang, A. J., Cummer, S. A., … Zhou, H. L. (2018). Observations of blue discharges associated with negative narrow bipolar events in active deep convection. *Geophys. Res. Lett.*, *45*(6), 2842–2851. https://doi.org/10.1002/2017GL076207

Liu, F. F., Zhu, B. Y., Lu, G. P., Lei, J. H., Shao, J., Chen, Y. L., Huang, A. J., Ma, M., Qin, Z. L., … Zhou, H. L. (2021a). Meteorological and electrical conditions of two mid-latitude thunderstorms producing blue discharges. *J. Geophys. Res: Atmos.*, *126*(8), e2020JD033648. https://doi.org/10.1029/2020JD033648

Liu, F. F., Lu, G. P., Neubert, T., Lei, J. H., Chanrion, O., Østgaard, N., Li, D. S., Luque, A., Gordillo-Vázquez, F. J., ... Zhu, B. Y. (2021b). Optical emissions associated with narrow bipolar events in radio signals from thunderstorm clouds penetrating into the stratosphere. *Nat. Commun.*, *12*(1), 6631. https://doi.org/10.1038/s41467-021-26914-4

Liu, F. F., Zhu, B. Y., Lu, G. P., and Ma, M. (2021c). Outbreak of negative narrow bipolar events in two mid-latitude thunderstorms featuring overshooting tops. *Remote Sens.*, *13*(24), 5130. https://doi.org/10.3390/rs13245130

Liu, H. Y., Dong, W. S., Wu, T., Zheng, D., and Zhang, Y. J. (2012). Observation of compact intracloud discharges using VHF broadband interferometers. *J. Geophys. Res.: Atmos.*, *117*(D1), D01203. https://doi.org/10.1029/2011JD016185

Lü, F. C., Zhu, B. Y., Zhou, H. L., Rakov, V. A., Xu, W. W., and Qin, Z. L. (2013). Observations of compact intracloud lightning discharges in the northernmost region (51°N) of China. *J. Geophys. Res.: Atmos.*, *118*(10), 4458–4465. https://doi.org/10.1002/jgrd.50295

Lyu, F. C., Cummer, S. A., Qin, Z. L., and Chen, M. L. (2019). Lightning initiation processes imaged with very high frequency broadband interferometry. *J. Geophys. Res.: Atmos.*, *124*(6), 2994–3004. https://doi.org/10.1029/2018JD029817

Ma, D. (2017). Characteristic pulse trains of preliminary breakdown in four isolated small thunderstorms. *J. Geophys. Res.: Atmos.*, *122*(6), 3361–3373. https://doi.org/10.1002/2016JD025899

Nag, A., and Rakov, V. A. (2010a). Compact intracloud lightning discharges: 1. Mechanism of electromagnetic radiation and modeling. *J. Geophys. Res.: Atmos.*, *115*(D20), D20102. https://doi.org/10.1029/2010JD014235

Nag, A., and Rakov, V. A. (2010b). Compact intracloud lightning discharges: 2. Estimation of electrical parameters. *J. Geophys. Res.: Atmos.*, *115*(D20), D20103. https://doi.org/10.1029/2010JD014237

Nag, A., Rakov, V. A., Tsalikis, D., and Cramer, J. A. (2010). On phenomenology of compact intracloud lightning discharges. *J. Geophys. Res.: Atmos.*, *115*(D14), D14115. https://doi.org/10.1029/2009JD012957

Neubert, T., Chanrion, O., Heumesser, M., Dimitriadou, K., Husbjerg, L., Rasmussen, I. L., Østgaard, N., and Reglero, V. (2021). Observation of the onset of a blue jet into the stratosphere. *Nature*, *589*(7842), 371–375. https://doi.org/10.1038/s41586-020-03122-6

Oetzel, G. N. (1968). Computation of the diameter of a lightning return stroke. *J. Geophys. Res.*, *73*(6), 1889–1896. https://doi.org/10.1029/JB073i006p01889

Qin, Z. L., Zhu, B. Y., Lü, F. C., Ma, M., and Ma, D. (2015). Using time domain waveforms of return strokes to retrieve the daytime fluctuation of ionospheric D layer. *Chin. Sci. Bull. (in Chinese)*, *60*(7), 654–663. https://doi.org/10.1360/n972014-00223

Rakov ,V. A., and Uman, M. A. (2003). *Lightning: Physics and Effects*. Cambridge: Cambridge University Press.

Rison, W., Krehbiel, P. R., Stock, M. G., Edens, H. E., Shao, X. M., Thomas, R. J., Stanley, M. A., and Zhang, Y. (2016). Observations of narrow bipolar events reveal how lightning is initiated in thunderstorms. *Nat. Commun.*, *7*(1), 10721. https://doi.org/10.1038/ncomms10721

Smith, D. A., Shao, X. M., Holden, D. N., Rhodes, C. T., Brook, M., Krehbiel, P. R., Stanley, M., Rison, W., and Thomas, R. J. (1999). A distinct class of isolated intracloud lightning discharges and their associated radio emissions. *J. Geophys. Res.: Atmos.*, *104*(D4), 4189–4212. https://doi.org/10.1029/1998JD200045

Smith, D. A., Heavner, M. J., Jacobson, A. R., Shao, X. M., Massey, R. S., Sheldon, R. J., and Wiens, K. C. (2004). A method for determining intracloud lightning and ionospheric heights from VLF/LF electric field records. *Radio Sci.*, *39*(1), RS1010. https://doi.org/10.1029/2002RS002790

Soler, S., Pérez-Invernón, F. J., Gordillo-Vázquez, F. J., Luque, A., Li, D., Malagón-Romero, A., Neubert, T., Chanrion, O., Reglero, V., Navarro-González, J., Lu, G., Zhang, H., Huang, A. (2020). Blue optical observations of narrow bipolar events by ASIM confirm streamer activity in thunderstorms. *J. Geophys. Res.: Atmos.*, 125 (2020). https://doi.org/10.1029/2020JD032708

Tilles, J. N., Liu, N. Y., Stanley, M. A., Krehbiel, P. R., Rison, W., Stock, M. G., Dwyer, J. R., Brown, R., and Wilson, J. (2019). Fast negative breakdown in thunderstorms. *Nat. Commun.*, *10*(1), 1648. https://doi.org/10.1038/s41467-019-09621-z

Watson, S. S., and Marshall, T. C. (2007). Current propagation model for a narrow bipolar pulse. *Geophys. Res. Lett.*, *34*(4), L04816. https://doi.org/10.1029/2006GL027426

Wiens, K. C., Hamlin, T., Harlin, J., and Suszcynsky, D. M. (2008). Relationships among Narrow Bipolar Events, ''total'' lightning, and radar-inferred convective strength in Great Plains thunderstorms. *J. Geophys. Res.: Atmos.*, *113*(D5), D05201. https://doi.org/10.1029/2007JD009400

Willett, J. C., Bailey, J. C., and Krider, E. P. (1989). A class of unusual lightning electric field waveforms with very strong high-frequency radiation. *J.*

Geophys. Res.: Atmos., *94*(D13), 16255–16267. https://doi.org/10.1029/JD094iD13p16255

Wu, T., Dong, W. S., Zhang, Y. J., and Wang, T. (2011). Comparison of positive and negative compact intracloud discharges. *J. Geophys. Res.: Atmos.*, *116*(D3), D03111. https://doi.org/10.1029/2010JD015233

Wu, T., Dong, W. S., Zhang, Y. J., Funaki, T., Yoshida, S., Morimoto, T., Ushio, T., and Kawasaki, Z. (2012). Discharge height of lightning narrow bipolar events. *J. Geophys. Res.: Atmos.*, *117*(D5), D05119. https://doi.org/10.1029/2011JD017054

Wu, T., Takayanagi, Y., Yoshida, S., Funaki, T., Ushio, T., and Kawasaki, Z. (2013). Spatial relationship between lightning narrow bipolar events and parent thunderstorms as revealed by phased array radar. *Geophys. Res. Lett.*, *40*(3), 618–623. https://doi.org/10.1002/grl.50112

Zhu, B. Y., Zhou, H. L., Ma, M., Lv, F. C., and Tao, S. C. (2010a). Estimation of channel characteristics of narrow bipolar events based on the transmission-line model. *J. Geophys. Res.: Atmos.*, *115*(D19), D19105. https://doi.org/10.1029/2009JD012021

Zhu, B. Y., Zhou, H. L., Ma, M., and Tao, S. C. (2010b). Observations of narrow bipolar events in East China. *J. Atmos. Sol. -Terr. Phys.*, *72*(2-3), 271–278. https://doi.org/10.1016/j.jastp.2009.12.002